Materials Advances

ROYAL SOCIETY OF CHEMISTRY

PAPER

Check for updates

Insight into the electron transfer and anti-thermal quenching of europium doped Li$_4$SrCa(SiO$_4$)$_2$†

Jieqi Hu, [ab] Philippe F. Smet, [a] Rik Van Deun [b] and David Van der Heggen *[a]

The understanding of lanthanide-related electron transfer processes is crucial for designing efficient and functional luminescent phosphors. However, the current knowledge on those processes between Eu ions with different oxidation states is rather scarce, which limits the progress of developing new efficient phosphors with good stability. In this work, we report on Eu^{2+}-doped Li$_4$SrCa(SiO$_4$)$_2$ and its solid solutions, in which optically-induced reversible electron transfer between Eu^{2+} and Eu^{3+} is demonstrated under illumination at different wavelengths. It is confirmed that the reversible electron transfer between Eu^{2+} and Eu^{3+} in inequivalent sites can be initiated by exciting the corresponding Eu^{2+}. Additionally, it is shown that the strong increase in orange emission intensity of Eu$_{Ca}^{2+}$ with temperature can be attributed to the thermally-assisted energy transfer from Eu$_{Sr}^{2+}$ to Eu$_{Ca}^{2+}$ and an increase of Eu$_{Ca}^{2+}$ centers due to photoinduced electron transfer. This phosphor was previously reported as a potential candidate for luminescence thermometry but, as shown here, the temperature-dependent, reversible electron transfer processes in combination with temperature-dependent energy transfer between Eu^{2+} ions on two different crystallographic sites would strongly compromise any attempt of measuring temperatures with this phosphor. The results of this work advance our understanding of electron transfer between Eu^{2+} and Eu^{3+} in general, which is very relevant for other europium doped phosphors.

Introduction

Lanthanide activators are widely used in luminescent materials.[1] As a commonly used lanthanide dopant, europium (Eu) can be incorporated in both divalent and trivalent oxidation states.[1] Even in phosphors that are intentionally doped with Eu^{2+}, the presence of Eu^{3+} is often unavoidable due to incomplete reduction during synthesis.[2–4] In certain cases, illumination of the phosphor can also result in optically-induced oxidation or reduction of Eu^{2+} and Eu^{3+}, respectively, due to an electron transfer between the activator ion and another dopant ion or intrinsic defect such as a vacancy.[4–7] If this electron transfer occurs between two metal ions differing only in oxidation state, the process is called intervalence charge transfer (IVCT).[8] However, such IVCT between Eu^{2+} and Eu^{3+} usually manifests itself as a quenching effect when the two Eu ions are incorporated on the same crystallographic site, or as so-called anomalous emission in a few exceptions, making it difficult to be identified.[9–11]

If the Eu ions are incorporated on two non-equivalent crystallographic sites, one may expect IVCT between Eu^{2+} and Eu^{3+} which will result in a change in emission color of the phosphor, because the emission spectrum originating from the 4f^{6}5d^1–4f^7 parity-allowed transitions of Eu^{2+} is highly sensitive to the local environment around Eu^{2+}.[1,12] This kind of IVCT and the accompanying change in luminescence has been reported in Li$_4$SrCa(SiO$_4$)$_2$:Eu^{2+} by Shi *et al.*[12] In Li$_4$SrCa(SiO$_4$)$_2$, there are two crystallographic sites available for Eu substitution, a Sr^{2+} site (CN = 10) with C_s symmetry in a coordination polyhedron of distorted bicapped square antiprisms, and a Ca^{2+} site (CN = 6) with C_2 symmetry in a smaller distorted octahedron (see Fig. S1, ESI†).[13] As reported in literature, Eu^{2+} ions prefer to occupy the Sr^{2+} site (denoted as Eu$_{Sr}^{2+}$) resulting in blue emission, while only a small fraction of Eu^{2+} ions are incorporated on the Ca^{2+} site (denoted as Eu$_{Ca}^{2+}$) resulting in orange emission.[12,14] Such preferential site occupation is also consistent with the fact that there is a smaller ionic radius difference between 10-coordinated Eu^{2+} (1.35 Å) and Sr^{2+} (1.36 Å), than between 6-coordinated Eu^{2+} (1.17 Å) and Ca^{2+} (1.0 Å).[15] Shi *et al.* reported that there is a substantial increase of Eu$_{Ca}^{2+}$-related orange emission and a simultaneous small decrease of Eu$_{Sr}^{2+}$-related blue emission if the sample is exposed to 330 nm illumination at an elevated temperature of 227 °C.[12] Moreover they showed that this optically induced change in luminescence is stable

a LumiLab, Department of Solid State Sciences, Ghent University, Krijgslaan 281-S1, 9000 Gent, Belgium. E-mail: david.vanderheggen@ugent.be

b L³, Department of Chemistry, Ghent University, Krijgslaan 281-S3, 9000 Gent, Belgium

† Electronic supplementary information (ESI) available. See DOI: https://doi.org/10.1039/d3ma00772c

under repeated heating and cooling of the material, provided that an equilibrium is reached under 330 nm illumination at 227 °C first. Based on these two properties it was claimed that Li$_4$SrCa(SiO$_4$)$_2$:Eu^{2+} can be exploited for temperature sensing based on the intensity ratio of the orange to blue emission under 330 nm excitation because the intensity ratio increases with temperature.[12] However, the origin of this increase was not discussed.[12] Unfortunately, the presented emission spectra for the temperature sensing are area-normalized, which obscures the analysis of the thermal quenching behaviour of Eu$_{Ca}^{2+}$ orange emission under 330 nm excitation.[12]

However, following the work of Shi *et al.*, the idea to apply Li$_4$SrCa(SiO$_4$)$_2$:Eu^{2+} for temperature sensing was adopted by Wu *et al.* using the same intensity ratio method but under 363 nm excitation.[16] They also found that the orange to blue intensity ratio increases with temperature, and the non-normalized emission spectra at different temperatures clearly show the anti-thermal quenching of Eu$_{Ca}^{2+}$ orange emission, *i.e.* an increase in emission intensity with temperature. In this case, the anti-thermal quenching was attributed to the temperature-dependent energy transfer, but the optically-induced electron transfer process, which also impacts the temperature-dependent luminescence, was not discussed. Recently, Su *et al.* exploited the luminescence properties of Li$_4$SrCa(SiO$_4$)$_2$:Eu^{2+} for pressure sensing based on the same intensity ratio method under excitation with a 355 nm laser.[17] Unfortunately, the influence of optically-induced electron transfer process during the measurement was not considered either.[17]

As a consequence, the effects of optical stimulation and temperature on the luminescence changes in Li$_4$SrCa(SiO$_4$)$_2$:Eu^{2+} are still only poorly understood as the two processes that affect it, *i.e.* energy transfer and electron transfer, have not yet been considered simultaneously. Moreover, the irreversibility of the charge transfer process reported by Shi *et al.* is in stark contrast to the behaviour of many other materials such as persistent phosphors like Sr$_4$Al$_{14}$O$_{25}$:Eu^{2+},Dy^{3+}, optically stimulated or thermally stimulated dosimeters like SrAl$_2$O$_4$:Eu^{2+},Sm^{3+} or photochromic materials like CaF$_2$:Eu^{2+},Sm^{3+} in which the charge transfer between defects is usually reversible if the material is heated to a sufficiently high temperature or exposed to stimulation light with a suitable wavelength.[5,12,18,19] Given that the applicability of this phosphor as an optical thermometer or pressure sensor highly depends on the stability of the charge transfer state, it is highly desirable that these charge and energy transfer processes are studied in more detail.

To study the electron transfer process responsible for the reduction and oxidation of the Eu dopant in this system, Li$_4$Sr$_{1+x}$Ca$_{1-x}$(SiO$_4$)$_2$:Eu^{2+} solid solutions were prepared. The influence of illumination wavelength, illumination time, illumination sequence and the role of temperature on the charge transfer between Eu^{2+} and Eu^{3+} were investigated in detail through photoluminescence and reflectance spectroscopy. Thermal quenching, thermally-assisted energy transfer and electron transfer are all considered at different temperatures to get a comprehensive understanding of the relevant processes at play in these materials.

Methods

Li$_4$Sr$_{0.99+x}$Ca$_{0.99-x}$(SiO$_4$)$_2$:0.02Eu^{2+} (x = −0.25, 0, 0.4) powders were synthesized by a high-temperature solid-state reaction, using high-purity Li$_2$CO$_3$ (Alfa Aesar, 99.998%), Sr$_2$CO$_3$ (Sigma Aldrich, 99.9%), CaCO$_3$ (Sigma Aldrich, 99.0%), SiO$_2$ (Alfa Aesar, 99.5%) and Eu$_2$O$_3$ (Alfa Aesar, 99.95%) as precursors. Stoichiometric mixtures of the precursors were weighed and ground and then precalcined at 700 °C in air for 6 h and finally fired at 920 °C for 6 h in a tube furnace under a flow of forming gas (10% H$_2$, 90% N$_2$). Then the product was naturally cooled to room temperature and slightly re-ground for further characterizations. A Li$_4$Sr$_{0.9975}$Ca$_{0.9975}$(SiO$_4$)$_2$:0.005Eu^{2+} sample with a lower doping concentration was also prepared by the same procedure. In addition, firing in air atmosphere, instead of a reducing atmosphere, was applied to prepare Eu^{3+} doped Li$_4$Sr$_{0.99}$Ca$_{0.99}$(SiO$_4$)$_2$:0.02Eu^{3+} while keeping other preparation conditions the same.

The phase purity was determined by X-ray diffraction (XRD) using a Siemens D5000 diffractometer (40 kV, 40 mA) with Cu K$_\alpha$ radiation (λ = 0.154 nm). From XRD peaks, lattice parameters were calculated using UnitCellWin software.[20] Photoluminescence (PL) emission and excitation (PLE) spectra of the sample were collected at room temperature using an Edinburgh Instrument FS920 fluorescence spectrometer equipped with a monochromated 450 W xenon arc lamp as excitation source. Low-temperature PL/PLE measurements were done inside a cryostat (Oxford Instruments Optistat CF). All spectra were corrected for detector response. To investigate the wavelength-dependent electron transfer, efficiency spectra for electron transfer are estimated by comparing the change of orange emission intensity before and after the illumination with the same number of incident photons with a certain wavelength. The efficiency of this process in the range of 300–430 nm for Li$_4$Sr$_{0.99+x}$Ca$_{0.99-x}$(SiO$_4$)$_2$:0.02Eu^{2+} (x = −0.25) was recorded using the monochromated xenon arc lamp from the FS920 spectrometer as the illumination source of different wavelengths. The same setup was used to record emission spectra upon excitation at 420 nm. The efficiency of the process in the range of 410–570 nm for Li$_4$Sr$_{0.99+x}$Ca$_{0.99-x}$(SiO$_4$)$_2$:0.02Eu^{2+} (x = 0.4) or 330 nm illuminated Li$_4$Sr$_{0.99+x}$Ca$_{0.99-x}$(SiO$_4$)$_2$:0.02Eu^{2+} (x = −0.25), was measured in a setup, having a wavelength-tunable OPO laser (Ekspla NT340), shutters, and a fiber-based detection (QE65000 spectrometer, Ocean Optics) of the emission spectra under 420 nm LED excitation. The intensity of the illumination light at the different wavelengths originating from the monochromated xenon arc lamp and the OPO laser was measured with a thermal power sensor (S401C, Thorlabs) and a pyroelectric energy sensor (ES220C, Thorlabs), respectively, to correct for the differences in illumination intensity. Measurements of the reflectance at 420 nm accompanied with recording the PL spectrum as a function of 365 nm LED illumination time under excitation with 365 nm LED or 420 nm LED, were performed in an experimental setup schematically depicted in Fig. S2 (ESI†), having two LEDs, two shutters and two spectrometers (QE65000, and AvaSpec-HERO, Avantes). Temperature-dependent PL under 365 nm or 420 nm LED excitation, were measured with a Linkam THMS600 temperature-controlled stage (60 °C min^{-1}) and

fiber-based detection setup. To minimize the effect of electron transfer resulted from excitation LED during temperature-dependent PL measurement, the shutter for the excitation LED was open only when necessary.

Results and discussion

To investigate the composition-dependent and concentration-dependent electron and energy transfer processes, $Li_4Sr_{0.99+x}$-$Ca_{0.99-x}(SiO_4)_2$:$0.02Eu^{2+}$ ($x = -0.25$, 0, 0.4) and $Li_4Sr_{0.9975}Ca_{0.9975}$-$(SiO_4)_2$:$0.005Eu^{2+}$ were prepared under a reducing atmosphere. Hereinafter, these compositions will be abbreviated as Ca-rich: 0.02Eu, Ca-Sr:0.02Eu, Sr-rich:0.02Eu, and Ca-Sr:0.005Eu, respectively. Other compositions with x outside the range of -0.25 to 0.4 could not be synthesized as impurity phases appear.[14] In addition, $Li_4Sr_{0.99}Ca_{0.99}(SiO_4)_2$:$0.02Eu^{3+}$ (abbreviated as Ca-Sr:0.02Eu (air)) was prepared in an air atmosphere to investigate the Eu^{3+} photoluminescence. As shown in Fig. 1a, the XRD patterns of all samples match well with the standard pattern of $Li_4SrCa(SiO_4)_2$ (JCPDS 83-0763). The corresponding lattice parameters increase with the Sr-content due to the larger ionic radius of Sr^{2+} than Ca^{2+} (Fig. 1b).

When prepared in air, Eu is incorporated in its trivalent oxidation state and low-temperature PL and PLE measurements allow to differentiate between Eu^{3+} ions incorporated on the two available sites (Fig. 2). Here Eu_{Ca}^{3+} gives rise to a prominent emission at 588.5 nm originating from the $^5D_0 \rightarrow {}^7F_1$ transition when excited by 250 nm, while an intense $^5D_0 \rightarrow {}^7F_4$ emission can be observed at 692.5 nm under 280 nm excitation which can be ascribed to Eu_{Sr}^{3+}.[12,21,22] Such a difference in Eu^{3+} luminescence is due to the difference in site symmetry, *i.e.* C_2 symmetry for Ca^{2+} site and C_s symmetry for Sr^{2+} site.[21] When a reducing atmosphere is used during the synthesis, two broad emission bands are observed in Ca-Sr:0.02Eu, each with a distinct excitation spectrum (Fig. 3a). Following the assignments by Shi *et al.*, the blue emission, peaking at 433 nm, is due to Eu_{Sr}^{2+} while the orange emission, peaking at 589 nm originates from Eu_{Ca}^{2+}. The coexistence of both emission bands is better visualized in Fig. 3b under 365 nm excitation, a wavelength which
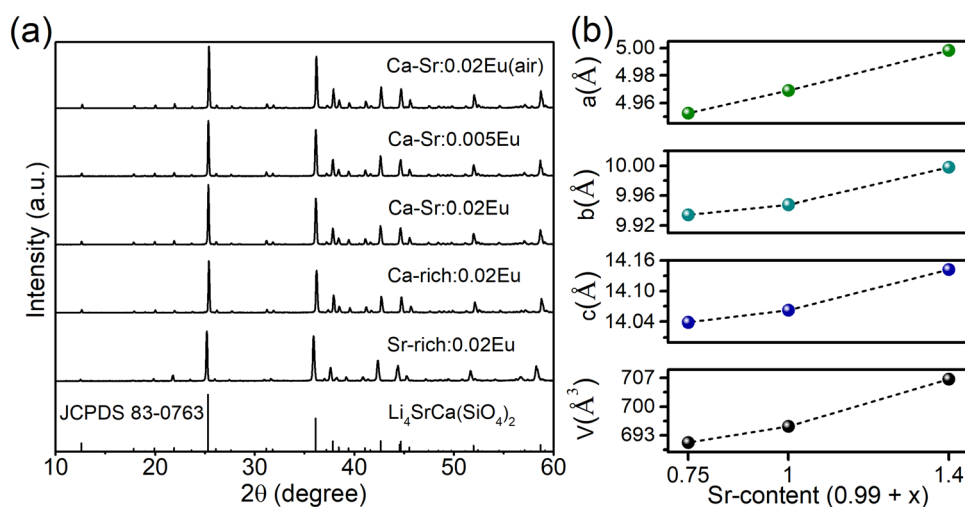

Fig. 1 (a) XRD patterns of all samples and the reference pattern of $Li_4SrCa(SiO_4)_2$ (JCPDS 83-0763). (b) The lattice parameters extracted from the XRD patterns for the samples prepared under a reducing atmosphere with 0.02Eu concentration.
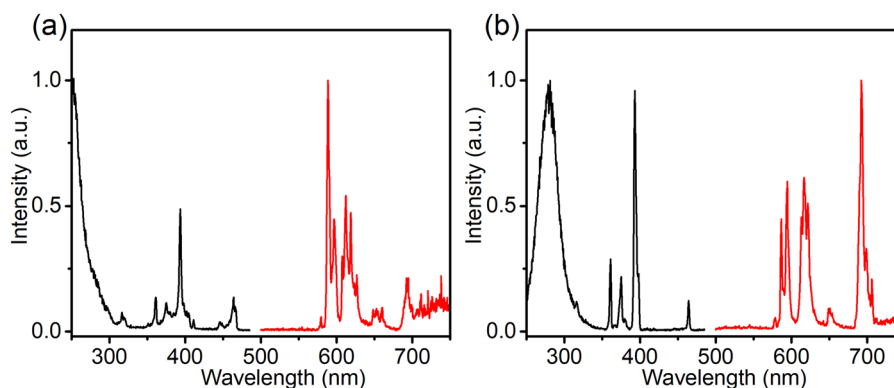

Fig. 2 Normalized PL and PLE spectra (at $-196\ °C$) of the Ca-Sr:0.02Eu (air) for (a) Eu_{Ca}^{3+} sites ($\lambda_{em} = 588.5$ nm; $\lambda_{ex} = 250.0$ nm) and (b) Eu_{Sr}^{3+} sites ($\lambda_{em} = 692.5$ nm; $\lambda_{ex} = 280.0$ nm).

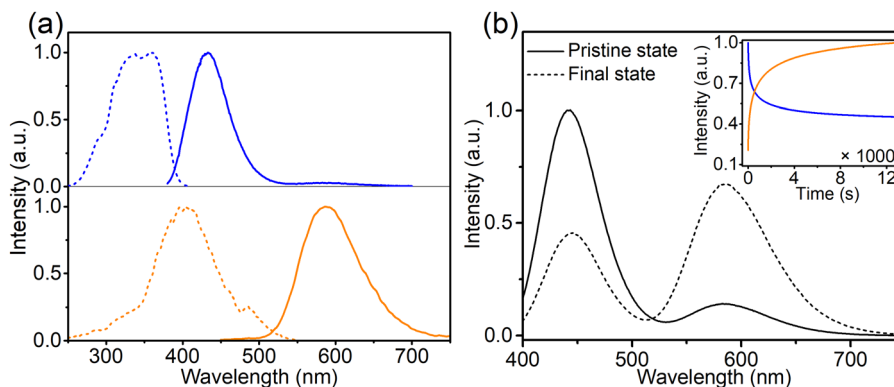**Fig. 3** (a) Normalized PL (—) and PLE (---) spectra of the Ca-Sr:0.02Eu for the blue (λ_{em}= 450 nm; λ_{ex} = 330 nm) and orange (λ_{em}= 589 nm; λ_{ex} = 420 nm) emission centers. (b) PL of the Ca-Sr:0.02Eu before and after 365 nm LED illumination under the excitation of the same LED. The inset shows the change of blue and orange emission intensities as a function of illumination time (pristine is taken at t = 0 s, while the final state is for t = 12 000 s).

predominantly excites Eu_{Sr}^{2+}. However, if we change the host composition to Ca-rich:0.02Eu, the orange emission is absent in the as-synthesized sample under 365 nm excitation and only the blue emission band is observed (Fig. 4a). On the contrary, in as-synthesized Sr-rich:0.02Eu, a pronounced orange emission band appears, even under 330 nm excitation which favors the excitation of the blue-emitting centers much more than the orange-emitting centers (Fig. 4b).[14] It hence appears that increasing the Ca-content suppresses the formation of orange-emitting Eu_{Ca}^{2+} centers during synthesis while an increase of Sr-content results in an increased formation of Eu_{Ca}^{2+} centers.[14]

The intensity of the two emission bands in Ca-Sr:0.02Eu exhibits a strong variation under continuous 365 nm excitation (3.8 mW cm^{-2}, inset of Fig. 3b). After 12 000 s of irradiation the intensities stabilize. The blue emission intensity has then decreased by roughly 50% while the orange emission intensity has increased dramatically by 380%. A similar evolution of the Eu^{2+} luminescence in $Li_4SrCa(SiO_4)_2$:Eu^{2+} has been reported by Shi *et al.* under illumination with 330 nm light at the elevated temperature of 227 °C, but they claimed that there is no detectable luminescence change when applying the same illumination at room temperature.[12] In contrast, here we demonstrate

that a similar effect can be achieved at room temperature even under illumination with lower energy photons. After the illumination is ended, the change is spontaneously reversed albeit relatively slowly at room temperature (Fig. S3, ESI†). If the material is heated to 200 °C, this reverse process can be accelerated (Fig. S3, ESI†). Both observations contradict the results by Shi *et al.*[12] One might argue that this is due to the different temperature at which the samples were illuminated. Hence the sample was exposed to 365 nm (2.8 mW cm^{-2}) at 227 °C for 20 min to induce the creation of Eu_{Ca}^{2+} centers and then kept at room temperature (60 min), 80 °C (30 min) and 200 °C (20 min). As shown in Fig. S4 (ESI†) also in this case the induced luminescence change is unstable.

This behaviour is also observed in Ca-rich:0.02Eu and Sr-rich0.02Eu samples, as will be shown later. This behaviour is very similar to what is encountered in many other inorganic luminescent or photochromic materials, such as CaF_2:Eu^{2+}, Sm^{3+}, $SrAl_2O_4$:Eu^{2+},Sm^{3+} and $Sr_4Al_{14}O_{25}$:Eu^{2+},Dy^{3+}.[5,18,19] In accordance with the widely accepted mechanisms in these materials, we propose a similar charge transfer process to explain the luminescence evolution:
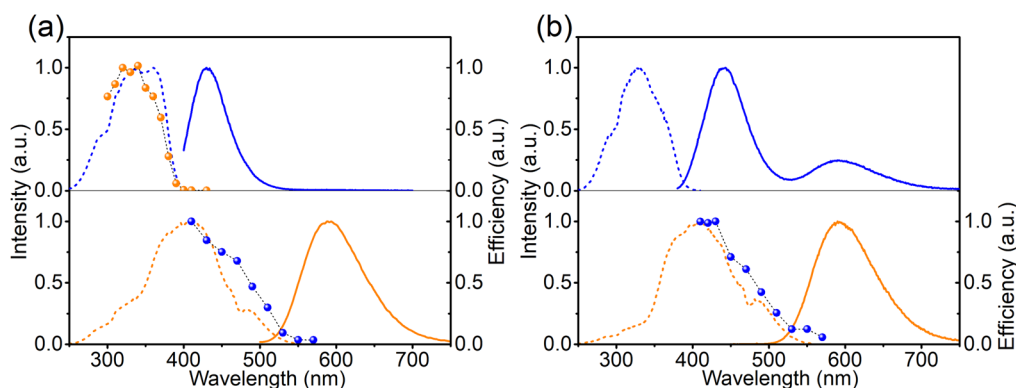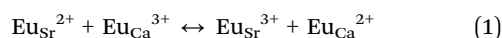
$$Eu_{Sr}^{2+} + Eu_{Ca}^{3+} \leftrightarrow Eu_{Sr}^{3+} + Eu_{Ca}^{2+} \qquad (1)$$

Fig. 4 (a) PLE (---) and PL (—) of as-synthesized Ca-rich:0.02Eu (blue lines, λ_{em}= 450 nm; λ_{ex} = 365 nm) and of Ca-rich:0.02Eu after 330 nm illumination (orange lines, λ_{em}= 589 nm; λ_{ex} = 420 nm). Electron transfer efficiency spectra for forward (orange spheres) and backward (blue spheres) electron transfer. (b) PLE (---) and PL (—) of as-synthesized Sr-rich:0.02Eu for the blue (λ_{em}= 450 nm; λ_{ex} = 330 nm) and orange (λ_{em}= 589 nm; λ_{ex} = 420 nm) emission centers, and the efficiency spectrum for backward electron transfer (blue spheres).

To study the mechanism behind the optically induced forward (from left to right in eqn (1)) or backward (from right to left in eqn (1)) charge transfer, the pristine Ca-rich:0.02Eu sample was exposed to light with different wavelengths but equal integrated intensities. The changes in Eu_{Ca}^{2+} concentration were monitored by recording the orange emission intensity under 420 nm excitation. Note that prior to the measurement for the backward charge transfer in Ca-rich:0.02Eu, the sample was illuminated by 330 nm for a sufficiently long time to maximize the concentration of Eu_{Ca}^{2+} ions as almost no Eu_{Ca}^{2+} centers are present in the as-synthesized material. As shown in Fig. 4a, the efficiency spectra for forward and backward charge transfer in Ca-rich:0.02Eu almost perfectly coincide with the PLE spectra of the involved divalent europium ions. Small discrepancies in the range of 340–370 nm can most likely be attributed to the overlap between the PLE of Eu_{Ca}^{2+} and Eu_{Sr}^{2+} which results in a competition between the two opposite directions of the reaction in eqn (1). This result indicates that the reaction in eqn (1) can be initiated in both directions through excitation of the involved divalent lanthanide ion. Similar results are obtained for the Sr-rich:0.02Eu (Fig. 4b) where the charge transfer efficiency spectrum for backward charge transfer coincides with the PLE of Eu_{Ca}^{2+} as well, suggesting the charge transfer can be achieved by exciting Eu_{Ca}^{2+}. The efficiency spectrum corresponding to the forward charge transfer of Sr-rich:0.02Eu is not measured, since the existing high concentration Eu_{Ca}^{2+} centers dramatically affects the recorded efficiency spectrum making it impossible to extract reliable information from the result. It should be emphasised that for the Sr-rich:0.02Eu most Eu_{Ca}^{2+} centers already exist in the as-synthesized sample, whereas for the Ca-rich:0.02Eu sample most of the Eu_{Ca}^{2+} centers are obtained by illumination. It can thus not *a priori* be assumed that both will behave in exactly the same way.

It is now clear that it is possible to change the ratio of blue to orange emission intensity in the as-synthesized materials by changing the composition of the host matrix. Naturally also the optically induced photoreduction and oxidation of the Eu ions are affected by the change in composition. If the as-synthesized samples are exposed to 330 nm light (Fig. 5a), thereby almost exclusively exciting the Eu_{Sr}^{2+}, the blue emission intensity decreases and simultaneously the orange emission increases in all compositions. This indicates that the reaction in eqn (1) proceeds in the forward direction, as expected. If the samples are subsequently exposed to 420 nm light which exclusively excites the Eu_{Ca}^{2+} centers, the changes are reversed indicating the reaction in eqn (1) proceeds in the backward direction.

If the sequence of illumination is changed (Fig. 5b), the situation is slightly more complicated. For the as-synthesized Ca-rich:0.02Eu and Ca-Sr:0.02Eu samples, illumination with 420 nm again induces an electron transfer from Eu_{Ca}^{2+} to Eu_{Sr}^{3+} although the changes are small due to the relatively small concentration of Eu_{Ca}^{2+}. However, in the Sr-rich:0.02Eu sample the decrease in orange emission intensity is not accompanied by an increase in blue emission. This can be understood by considering that the reaction in eqn (1) can only occur in the backward direction if there are sufficient Eu_{Sr}^{3+}. The existence of a large fraction of Eu^{3+} in $Li_4SrCa(SiO_4)_2:Eu^{2+}$ has previously been confirmed using X-ray absorption near-edge structure measurement, however, site-selective PL spectroscopy suggested a preferential occupation of Eu^{3+} on Ca^{2+} sites in $Li_4SrCa(SiO_4)_2:Eu^{3+}$.[12,15] In addition, Zhang *et al.* has reported the presence of narrow Eu^{3+} emission at 589 and 611 nm in $Li_4Ca_{0.8}Sr_{1.16}(SiO_4)_2:0.04Eu^{2+}$, which can be ascribed to Eu_{Ca}^{3+} according to our previous analysis in Fig. 2.[14] Also here only emission related to Eu_{Ca}^{3+} could be identified in the as-synthesized Sr-rich:0.02Eu (Fig. S5, ESI†). This suggest that the redox reaction in eqn (1) cannot proceed in the backward direction due to a shortage of Eu_{Sr}^{3+} centers in the as-synthesized Sr-rich:0.02Eu. Hence, another defect acts as an electron trapping center. Unfortunately, the chemical nature of this defect remains unknown at the moment. We also evaluated the repeatability of electron transfer process by alternating 330 nm and 420 nm illumination for multiple cycles, and the variations of orange emission shown in Fig. S6 (ESI†) convince us that electron transfer process is optically reversible with good repeatability for all the samples.

For the sake of completeness, the behaviour of all samples under illumination with 365 nm LED (7.93 mW cm^{-2}), close to the wavelength of 363 nm employed by Wu *et al.*, was also investigated (Fig. 6a and b).[16] At this wavelength both sites are excited with a comparable efficiency (Fig. 3 and 4). Hence, the direction in which the reaction in eqn (1) will proceed will be determined by the initial
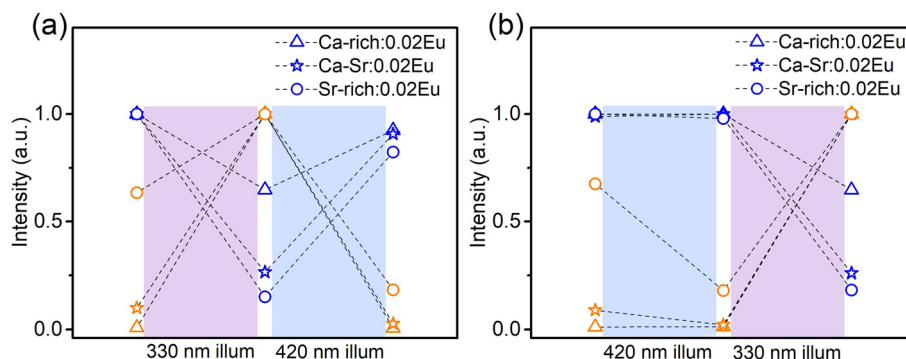

Fig. 5 Variation of blue and orange emissions excited using 365 nm light after illumination in a sequence of (a) 330 nm then 420 nm or (b) 420 nm then 330 nm for sufficiently long time, until saturation.

concentrations of Eu_{Sr}^{2+} and Eu_{Ca}^{2+} centers in the as-synthesized samples and will result in a decrease of the most abundant species. In the Ca-rich:0.02Eu and Ca-Sr:0.02Eu samples, illumination with 365 nm light will mainly excite Eu_{Sr}^{2+} centers and hence the behaviour is similar to that under exposure to 330 nm light. In contrast, in the Sr-rich:0.02Eu sample mostly Eu_{Ca}^{2+} centers will be excited and hence the behaviour is similar to that encountered under illumination with 420 nm light.

Apart from varying compositions also the influence of doping concentration was investigated (Fig. 6c and d) by comparing the photoredox processes for Ca-Sr:0.005Eu and Ca-Sr:0.02Eu. The increase of both orange emission intensity and the absorption at 420 nm (Fig. S7b, ESI†) are much more evident in Ca-Sr:0.02Eu than in Ca-Sr:0.005Eu. Therefore, it is safe to conclude that a higher doping concentration leads to the formation of more Eu_{Ca}^{2+} centers when the same 365 nm illumination process is applied. This concentration dependency might also offer an explanation why Shi *et al.* did not observe any charge transfer under 330 nm illumination at room temperature as the doping concentration in their sample is 60% lower than the concentration used here.[12] However, the intensity of the illumination light might also play a role since a high power 365 nm LED was used in our case while they only used monochromated 330 nm from Xe lamp.[12]

To construct a more detailed picture of electron transfer, and to facilitate the analysis of the following thermal quenching (TQ) behaviour, the effect of temperature on the photo-redox efficiency was investigated (Fig. 7 and Fig. S8, ESI†). After 365 nm (2.8 mW cm^{-2}) illumination at 227 °C, the orange

emission of Ca-Sr:0.02Eu significantly increased by a factor of 8.6 (Fig. 7a), while the same illumination at room temperature only resulted in an increase by a factor of two (Fig. 7a), thus confirming a strong temperature dependency of the forward electron transfer in eqn (1). To test the thermal activation of the backward charge transfer, the Ca-Sr:0.02Eu sample was first illuminated with 365 nm LED for 40 min at room temperature to maximize the orange emission intensity and then kept in the dark at room temperature for another 40 min to minimize the effects of fading after which the sample was subjected to three different treatments. If the sample was exposed to 490 nm light (21 mW cm^{-2}) for 3.5 min at room temperature, the orange emission decreased by only 6.6% (Fig. 7b). If this illumination was carried out at 227 °C, the decrease in orange emission intensity amounted to 25.9% (Fig. 7b) whereas only a decrease of 14.8% (Fig. 7b) was obtained if the sample was kept at 227 °C without any illumination. Clearly the change upon illumination at an elevated temperature is substantially larger than the sum of the two separate processes, *i.e.* illumination at room temperature or an elevated temperature without illumination, thereby confirming the existence of thermal activation of the backward charge transfer. However, the effect is much smaller compared to the forward charge transfer. The temperature dependency of electron transfer, as we have shown above, is similar to what has been observed in some persistent phosphors where there is a thermal barrier for charge trapping, for example in $Sr_2MgSi_2O_7$:Eu^{2+},Dy^{3+} or in $SrAl_2O_4$:Eu^{2+},Dy^{3+}.[23–25]

The TQ profiles (Fig. 8) for all samples were recorded under excitation with 365 nm light (exciting both orange and blue
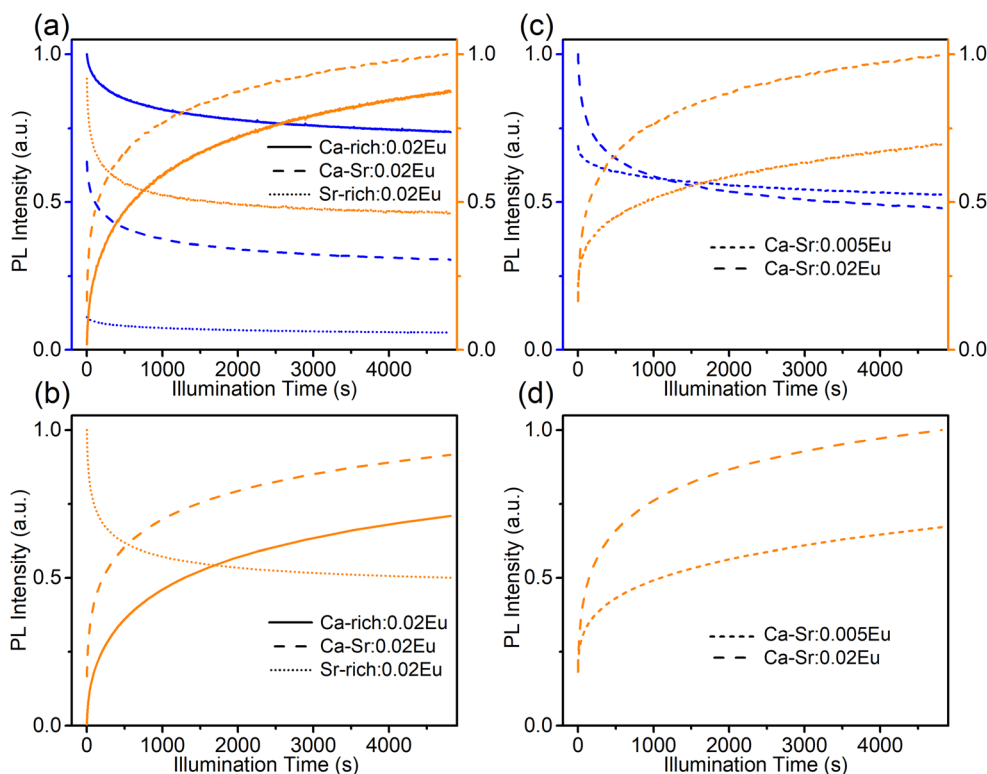

Fig. 6 Variation of blue (blue lines) and orange (orange lines) emissions over time under continuous 365 nm illumination using 365 nm light (a) and (c) or 420 nm light (b) and (d) to excite the luminescence in different samples.
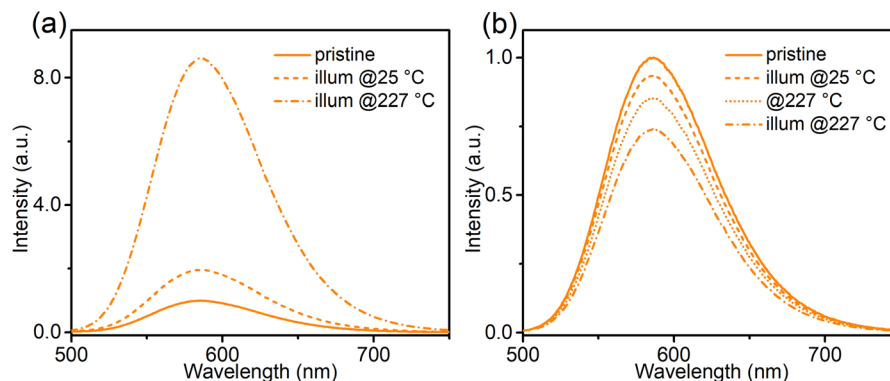
Fig. 7 (a) The orange emission spectra (λ_{ex} = 420 nm, all recorded at 25 °C) of Ca-Sr:0.02Eu in as-prepared state (solid curve), and after illumination (365 nm LED, 2 min) at 25 °C or at 227 °C separately. (b) Ca-Sr:0.02Eu was firstly illuminated with 365 nm LED (40 min, 25 °C) and then kept in dark (40 min, 25 °C). The emission spectra (λ_{ex} = 420 nm, 25 °C) of this treated state (solid curve), and the state with additional treatment by illumination (490 nm LED, 3.5 min, 25 °C) or annealing (3.5 min, 227 °C), or illumination at high temperature (490 nm LED, 3.5 min, 227 °C) separately.

emission) and 420 nm light (exciting only the orange emission, Fig. 8f) while heating at a rate of 60 °C min^{-1}. The corresponding emission spectra are shown in Fig. S9 and S10 (ESI†). The TQ profiles of the blue emission recorded under 365 nm excitation show a conventional behaviour with a quenching temperature $T_{0.5}$ of 160 °C for Ca-rich:0.02Eu, Ca-Sr:0.005Eu and Ca-Sr:0.02Eu and a slightly lower temperature of only 148 °C for Sr-rich:0.02Eu. In contrast, the orange emission intensity under 365 nm excitation increases with temperature for all samples except for Sr-rich:0.02Eu. This unusual anti-thermal quenching behaviour is a consequence of

temperature-dependent energy transfer from the blue-emitting Eu_{Sr}^{2+} centres to the orange-emitting Eu_{Ca}^{2+} centres in combination with an increase of Eu_{Ca}^{2+} centers due to the photoinduced charge transfer upon 365 nm excitation. The latter can be attributed to the forward electron transfer shown in eqn (1), which is inevitable, especially at elevated temperatures where the process proceeds with a higher efficiency as shown in Fig. 7a. The contribution of the charge transfer to the increase in intensity was quantified by measuring the orange and blue emission intensities after cooling down to room temperature again.
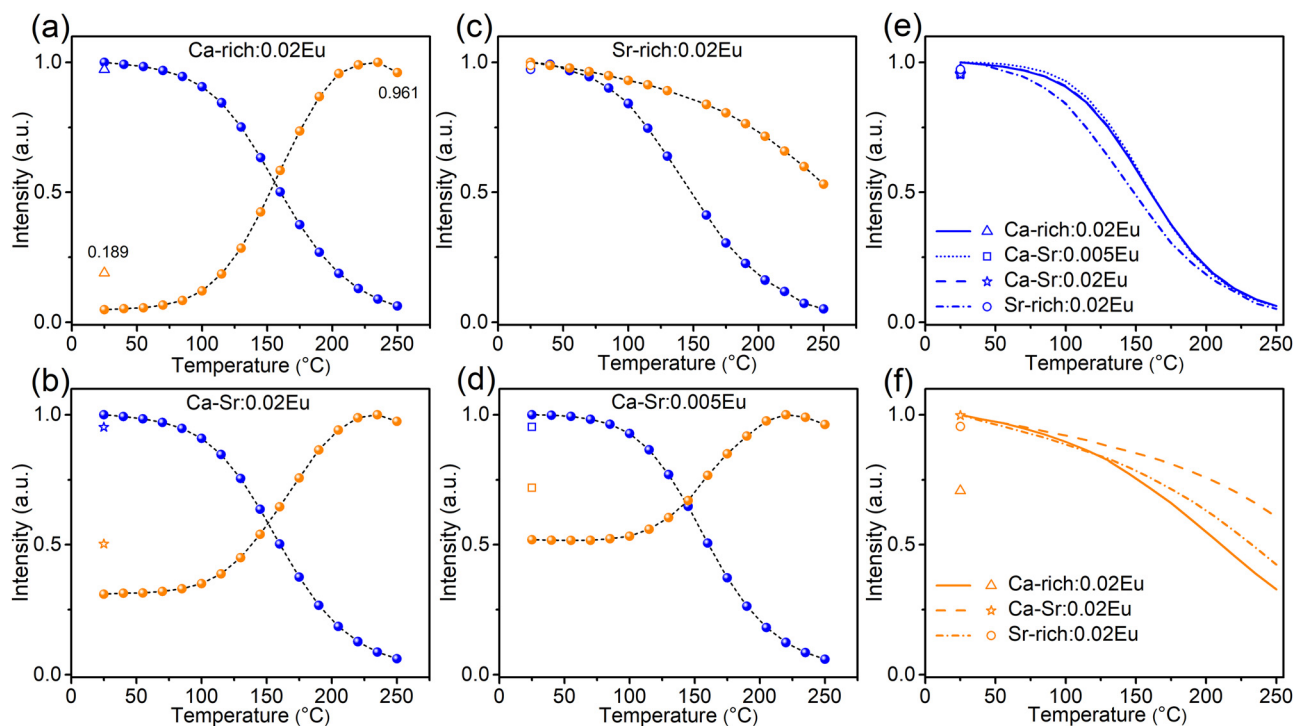

Fig. 8 Thermal quenching profiles of blue emission (blue curves) and orange emission (orange curves) in Ca-rich:0.02Eu (a), Ca-Sr:0.02Eu (b), Sr-rich:0.02Eu (c), Ca-Sr:0.005Eu (d) recorded under 365 nm LED excitation while heating at a rate of 60 °C min^{-1}. The results for the blue emission are summarized in (e). (f) Thermal quenching profiles of orange emission recorded under 420 nm LED excitation while heating at a rate of 60 °C min^{-1}. Ca-rich:0.02Eu in (f) was pre-illuminated by 365 nm LED for 1.5 h and then kept in the dark at room temperature for 1.5 h because there is no orange emission in the as-synthesized material. The emission intensity after cooling back to 25 °C (without illumination during cooldown) was also recorded and is shown using the symbol in each figure.

However, the optically-induced electron transfer only contributes to a small extent to such anti-thermal quenching of Eu_{Ca}^{2+} under 365 nm excitation shown in Fig. 8a, b and d. This can be substantiated by considering the situation of Ca-rich:0.02Eu in Fig. 8a as an example. If the TQ is recorded under excitation with 420 nm light (Fig. 8f), thereby only exciting the orange emission, the intensity decreases to 33% of the original intensity when heated to 250 °C. After the sample is cooled down (without illumination) to 25 °C it can be observed that the orange emission intensity has dropped to 71% of the intensity recorded prior to the TQ measurement indicating that the concentration of Eu_{Ca}^{2+} centres has decreased due to the illumination with 420 nm at an elevated temperature. Assuming a linear decrease in concentration during the measurement, the TQ profile can be corrected to isolate the actual quenching behaviour of the orange emission centre as shown in Fig. S11 (ESI†). This information can subsequently be used to correct the TQ curve recorded under 365 nm excitation (Fig. S11, ESI†) for the quenching of the orange emission centre. It can then be seen that the orange emission intensity doubles when heating to 250 °C while the Eu_{Ca}^{2+} concentration increases by only 19% as a consequence of the illumination with 365 nm light as evidenced by a PL measurement at 25 °C after the TQ measurement. Hence it can safely be concluded that the electron transfer only slightly contributes to the anti-thermal quenching of Eu_{Ca}^{2+}, and that thermally-assisted energy transfer is the driving force for the increase in intensity with temperature. A similar reasoning holds for Ca-Sr:0.02Eu and Ca-Sr:0.005Eu. The different behaviour of the Sr-rich:0.02Eu sample (Fig. 8c) can be understood by considering that the relatively low concentration of Eu_{Sr}^{2+} centers minimizes both the energy transfer and the charge transfer mechanisms that dominate in the other samples.

At the same time, the energy transfer is rather limited at room temperature even though there is an overlap between the PLE spectrum of Eu_{Ca}^{2+} and the PL spectrum of Eu_{Sr}^{2+}. This can be deduced as follows. In Fig. 5, the numbers of Eu_{Ca}^{2+} centres and Eu_{Sr}^{2+} centers change considerably during 330 nm/420 nm illumination, which will definitely alter the ratio of energy donors (Eu_{Sr}^{2+}) to energy acceptors (Eu_{Ca}^{2+}). This then consequently changes the contribution of energy transfer for orange emission under 365 nm excitation. However, if 420 nm light is used to exclusively excite Eu_{Ca}^{2+} centers during the same illumination process, the obtained orange emission intensity variations (Fig. S12, ESI†) are almost the same as the results shown in Fig. 5, thus confirming the limited energy transfer between Eu_{Sr}^{2+} and Eu_{Ca}^{2+} at room temperature. However, with increasing temperature the energy transfer is greatly enhanced, which leads to the unusual thermal behavior of Eu_{Ca}^{2+} shown in Fig. 8. Energy transfer between non-equivalent Eu^{2+} ions is a very common phenomenon for the phosphors in which Eu^{2+} is incorporated on non-equivalent sites, such as in $SrAl_2O_4$:Eu^{2+}, $Sr_4Al_{14}O_{25}$:Eu^{2+}, $Sr_5(PO_4)_{3-x}(BO_3)_x$Cl:Eu^{2+} ($x = 0$–0.7), $Ca_6BaP_4O_{17}$:Eu^{2+}, $RbBaPO_4$:Eu^{2+}, $Sr_5SiO_4Cl_6$:Eu^{2+}, $Ba_4Gd_3Na_3(PO_4)_6F_2$:Eu^{2+} [25–35] However, the detailed investigation of the temperature dependency of such energy transfer is very scarce. In the case of $Li_4Sr_{1+x}Ca_{1-x}(SiO_4)_2$:Eu, there are two possible explanations for the temperature dependency of the energy transfer. A first possibility is an increased spectral overlap between the Eu_{Sr}^{2+} emission and Eu_{Ca}^{2+} absorption bands due to thermal broadening. [27,28,36] Secondly, it is possible that higher temperatures promote the excitation energy migration from one Eu_{Sr}^{2+} ion to another which is finally followed by energy transfer to a Eu_{Ca}^{2+} ion. [36–38] This type of diffusion-limited energy migration can result in a similar temperature dependency. However, based on the available data, it is not possible to differentiate between these two possibilities. Usually, the energy transfer process is concentration dependent. [36] By comparing the TQ curves of Ca-Sr:0.02Eu and Ca-Sr:0.005Eu, which differ only in doping concentration (Fig. 8b and d), it can be seen that this concentration dependency is also demonstrated here as the orange emission intensity increases more at high temperature if the dopant concentration is increased. All in all, the results shown in Fig. 8 demonstrate how the excitation wavelength, the host composition and the doping concentration of Eu impact the thermal behaviour of Eu^{2+} orange emission from the perspective of thermally-activated characteristic of both electron transfer and energy transfer, which might be instructive to develop so-called zero- or anti-thermal quenching phosphors. [39–44]

Conclusion

A series of Eu^{2+} doped $Li_4Sr_{1+x}Ca_{1-x}(SiO_4)_2$ ($x = -0.25, 0, 0.4$) with blue-emitting Eu_{Sr}^{2+} and orange-emitting Eu_{Ca}^{2+} were prepared. By varying the relative contents of Sr and Ca, the occupation preference of Eu^{2+} on Sr^{2+} and Ca^{2+} sites can be regulated, thus the emission colour can be tuned. Moreover, illumination at different wavelengths, which induces reversible electron transfers between Eu^{2+} and Eu^{3+}, is also effective in changing the emission spectra of the as-prepared samples in a desired way. Based on the electron transfer efficiency spectra it can be concluded that the electron transfer from Eu_{Sr}^{2+} to Eu_{Ca}^{3+} can be initiated by exciting Eu_{Sr}^{2+}, while the reverse process can be initiated by exciting Eu_{Ca}^{2+}. Both these processes are temperature-dependent, according to the performed temperature-dependent illumination experiments. Unusual thermal quenching of orange emission was observed in Ca-rich:0.02Eu, Ca-Sr:0.02Eu and Ca-Sr:0.005Eu samples under 365 nm LED excitation. This can be explained mainly by thermally-assisted energy transfer from Eu_{Sr}^{2+} to Eu_{Ca}^{2+}. Thermally-assisted electron transfer from Eu_{Sr}^{2+} to Eu_{Ca}^{2+} also contributes to such behaviour, but to a lesser extent. Such uncommon thermal quenching was not observed in Sr-rich:0.02Eu due to the lack of Eu_{Sr}^{2+}. The concentration dependency of the electron transfer is also confirmed by comparing the illumination response of Ca-Sr:0.02Eu and Ca-Sr:0.005Eu. Cycling measurements by alternatively inducing forward and backward electron transfer suggest good repeatability of the electron transfer behaviour. Overall it can be concluded that the photo-induced and temperature-dependent luminescence changes in $Li_4Sr_{1+x}Ca_{1-x}(SiO_4)_2$:Eu result in a complicated behaviour which should be carefully considered before proposing the use of this phosphor in temperature and pressure sensing applications. Finally, such an electron transfer process may not be limited to Eu^{2+} and Eu^{3+} in inequivalent sites, similar processes between Sm^{2+} and Sm^{3+} probably occur in $Li_4Sr_{1+x}Ca_{1-x}(SiO_4)_2$ as well.

Conflicts of interest

There are no conflicts to declare.

Acknowledgements

References

1 G. Blasse and B. C. Grabmaier, *Luminescent Materials*, Springer-Verlag, 1994.

2 S. X. Li, L. Wang, D. M. Tang, Y. Cho, X. J. Liu, X. T. Zhou, L. Lu, L. Zhang, T. Takeda, N. Hirosaki and R.-J. Xie, *Chem. Mater.*, 2018, **30**(2), 494–505.

3 J. Qiao, S. Zhang, X. Zhou, W. Chen, R. Gautier and Z. Xia, *Adv. Mater.*, 2022, **34**(26), 2201887.

4 L. Amidani, K. Korthout, J. J. Joos, M. van der Linden, H. F. Sijbom, A. Meijerink, D. Poelman, P. F. Smet and P. Glatzel, *Chem. Mater.*, 2017, **29**, 10122–10129.

5 J. J. Joos, K. Korthout, L. Amidani, P. Glatzel, D. Poelman and P. F. Smet, *Phys. Rev. Lett.*, 2020, **125**, 033001.

6 J. Hu, Z. Yang, A. Feng, R. Deun Van, P. F. Smet and D. Van der Heggen, *J. Phys. Chem. C*, 2022, **126**, 21396–21404.

7 M. A. Van De Haar, M. Tachikirt, A. C. Berends, M. R. Krames, A. Meijerink and F. T. Rabouw, *ACS Photonics*, 2021, **8**(6), 1784–1793.

8 Z. Barandiaran, A. Meijerink and L. Seijo, *Phys. Chem. Chem. Phys.*, 2015, **17**, 19874.

9 C. MacKeen, F. Bridges, M. Kozina, A. Mehta, M. F. Reid, J.-P. R. Wells and Z. Barandiarán, *J. Phys. Chem. Lett.*, 2017, **8**, 3313–3316.

10 P. Dorenbos, *J. Phys.: Condens. Matter*, 2003, **15**(17), 2645–2665.

11 J. J. Joos, L. Seijo and Z. Barandiarán, *J. Phys. Chem. Lett.*, 2019, **10**, 1581–1586.

12 R. Shi, L. Ning, Y. Huang, Y. Tao, L. Zheng, Z. Li and H. Liang, *ACS Appl. Mater. Interfaces*, 2019, **11**, 9691–9695.

13 A. Akella and D. A. Keszler, *Inorg. Chem.*, 1995, **34**, 1308–1310.

14 J. Zhang, Z. H. Hua and S. Z. Wen, *Opt. Mater. Express*, 2015, **5**, 1704–1714.

15 R. D. Shannon, *Acta Crystallogr., Sect. A: Cryst. Phys., Diffr., Theor. Gen. Crystallogr.*, 1976, **32**, 751–767.

16 M. Wu, D. Deng, F. Ruan, B. Chen and S. Xu, *Chem. Eng. J.*, 2020, **396**, 125178.

17 K. Su, L. Mei, Q. Guo, P. Shuai, Y. Wang, Y. Liu, Y. Jiang, Z. Peng, B. Zou and L. Liao, *Adv. Funct. Mater.*, 2022, 2305359.

18 D. Van der Heggen, R. Zilenaite, E. Ezerskyte, V. Fritz, K. Korthout, D. Vandenberghe, J. De Grave, J. Garrevoet, L. Vincze, D. Poelman, J. J. Joos and P. F. Smet, *Adv. Funct. Mater.*, 2022, **32**, 2109635.

19 J. J. Joos, D. Van der Heggen, L. Amidani, L. Seijo and Z. Barandiarán, *Phys. Rev. B: Condens. Matter Mater. Phys.*, 2021, **104**, L201108.

20 T. J. B. Holland and S. A. T. Redfern, *Mineral. Mag.*, 1997, **61**, 65–77.

21 K. Binnemans, *Coord. Chem. Rev.*, 2015, **295**, 1–45.

22 F. J. Avella, O. J. Sovers and C. S. Wiggins, *J. Electrochem. Soc.*, 1967, **114**, 613.

23 C. Tydtgat, K. W. Meert, D. Poelman and P. F. Smet, *Opt. Mater. Express*, 2016, **6**, 844–858.

24 A. Feng, J. J. Joos, J. Du and P. F. Smet, *Phys. Rev. B: Condens. Matter Mater. Phys.*, 2022, **105**(20), 205101.

25 J. Botterman, J. J. Joos and P. F. Smet, *Phys. Rev. B: Condens. Matter Mater. Phys.*, 2014, **90**, 085147.

26 G. Blasse, *J. Solid State Chem.*, 1986, **62**, 207–211.

27 J. Bierwagen, S. Yoon, N. Gartmann, B. Walfort and H. Hagemann, *Opt. Mater. Express*, 2016, **6**, 793–803.

28 D. Dutczak, T. Jüstel, C. Ronda and A. Meijerink, *Phys. Chem. Chem. Phys.*, 2015, **17**, 15236–15249.

29 B. Smets, J. Rutten, G. Hoeks and J. Verlijsdonk, *J. Electrochem. Soc.*, 1989, **136**, 2119.

30 P.-P. Dai, C. Li, X.-T. Zhang, J. Xu, X. Chen, X.-L. Wang, Y. Jia, X. Wang and Y.-C. Liu, *Light: Sci. Appl.*, 2016, **5**, e16024.

31 R. Zhou, C. Liu, L. Lin, Y. Huang and H. Liang, *Chem. Eng. J.*, 2019, **369**, 376–385.

32 R. F. Zhou, F. K. Ma, F. Su, Y. Y. Ou, Z. M. Qi, J. H. Zhang, Y. Huang, P. Dorenbos and H. B. Liang, *Inorg. Chem.*, 2020, **59**, 17421–17429.

33 S. Dutta, S. Som, M. L. Meena, R. Chaurasiya and T. M. Chen, *Inorg. Chem.*, 2020, **59**(3), 1928–1939.

34 X. Fu, W. Lü, M. Jiao and H. You, *Inorg. Chem.*, 2016, **55**, 6107–6113.

35 S. Asaithambi, J. Lee, J.-W. Lee, B. D. Lee, M.-Y. Cho, W. B. Park and K.-S. Sohn, *J. Lumin.*, 2023, **263**, 120109.

36 P. A. Tanner, L. Zhou, C. Duan and K.-L. Wong, *Chem. Soc. Rev.*, 2018, **47**, 5234–5265.

37 J. C. Bourcet and F. K. Fong, *J. Chem. Phys.*, 1974, **60**, 34–39.

38 V. Bachmann, C. Ronda and A. Meijerink, *Chem. Mater.*, 2009, **21**(10), 2077–2084.

39 Y. H. Kim, P. Arunkumar, B. Y. Kim, S. Unithrattil, E. Kim, S. H. Moon, J. Y. Hyun, K. H. Kim, D. Lee, J. S. Lee and W. B. Im, *Nat. Mater.*, 2017, **16**, 543–550.

40 J. W. Qiao, L. X. Ning, M. S. Molokeev, Y. C. Chuang, Q. L. Liu and Z. G. Xia, *J. Am. Chem. Soc.*, 2018, **140**, 9730–9736.

41 P. Dang, W. Wang, H. Lian, G. Li and J. Lin, *Adv. Opt. Mater.*, 2022, **10**, 2102287.

42 M. Hermus, P.-C. Phan, A. C. Duke and J. Brgoch, *Chem. Mater.*, 2017, **29**, 5267–5275.

43 L. Huang, Y. Wei, Y. Pan, E. Zhou, Z. Yuan, H. Song, Y. Wang, J. Zhou, J. Rui, M. Xu, L. Ning, Z. Liu, H. Wang, X. Xie, X. Tang, H. Su and X. Xing, *Angew. Chem., Int. Ed.*, 2023, **135**(27), e202303482.

44 H. Zou, X. Yang, B. Chen, Y. Du, B. Ren, X. Sun, X. Qiao, Q. Zhang and F. Wang, *Angew. Chem., Int. Ed.*, 2019, **58**(48), 17255–17259.